Discovery of amivantamab (JNJ-61186372), a bispecific antibody targeting EGFR and MET

Neijssen, J.; Cardoso, R.M.F.; Chevalier, K.M.; Wiegman, L.; Valerius, T.; Anderson, G.M.; ... ; Chiu, M.L.

JBC RESEARCH ARTICLE

Discovery of amivantamab (JNJ-61186372), a bispecific antibody targeting EGFR and MET

Received for publication, October 26, 2020, and in revised form, March 4, 2021 Published, Papers in Press, April 8, 2021,
https://doi.org/10.1016/j.jbc.2021.100641

Joost Neijssen[1,‡], Rosa M. F. Cardoso[2,‡], Kristen M. Chevalier[2], Luus Wiegman[1], Thomas Valerius[3], G. Mark Anderson[2], Sheri L. Moores[2], Janine Schuurman[1], Paul W. H. I. Parren[1], William R. Strohl[2], and Mark L. Chiu[2,*]

From the [1]Genmab, Utrecht, The Netherlands; [2]Janssen Research & Development, Spring House, Pennsylvania, USA; [3]Section for Stem Cell Transplantation and Immunotherapy, Department of Medicine II, Christian Albrechts University and University Hospital Schleswig-Holstein, Kiel, Germany

Edited by Peter Cresswell

A bispecific antibody (BsAb) targeting the epidermal growth factor receptor (EGFR) and mesenchymal–epithelial transition factor (MET) pathways represents a novel approach to overcome resistance to targeted therapies in patients with non–small cell lung cancer. In this study, we sequentially screened a panel of BsAbs in a combinatorial approach to select the optimal bispecific molecule. The BsAbs were derived from different EGFR and MET parental monoclonal antibodies. Initially, molecules were screened for EGFR and MET binding on tumor cell lines and lack of agonistic activity toward MET. Hits were identified and further screened based on their potential to induce untoward cell proliferation and cross-phosphorylation of EGFR by MET *via* receptor colocalization in the absence of ligand. After the final step, we selected the EGFR and MET arms for the lead BsAb and added low fucose Fc engineering to generate amivantamab (JNJ-61186372). The crystal structure of the anti-MET Fab of amivantamab bound to MET was solved, and the interaction between the two molecules in atomic details was elucidated. Amivantamab antagonized the hepatocyte growth factor (HGF)-induced signaling by binding to MET Sema domain and thereby blocking HGF β-chain—Sema engagement. The amivantamab EGFR epitope was mapped to EGFR domain III and residues K443, K465, I467, and S468. Furthermore, amivantamab showed superior antitumor activity over small molecule EGFR and MET inhibitors in the HCC827-HGF *in vivo* model. Based on its unique mode of action, amivantamab may provide benefit to patients with malignancies associated with aberrant EGFR and MET signaling.

Aberrant activations of both epidermal growth factor receptor (EGFR) and mesenchymal–epithelial transition factor (MET) signaling pathways have been implicated in driving tumor cell growth and proliferation in lung cancer (1–4). In a subgroup of non–small cell lung cancer (NSCLC), activating mutations in the *EGFR* gene, mainly L858R mutation and exon 19 deletions, result in ligand-independent activation of the EGFR kinase activity (5). Tyrosine kinase inhibitors (TKIs) targeting EGFR are the standard of care for patients with EGFR-mutated NSCLC (6, 7); however, many patients will acquire resistance to TKIs (8, 9). In addition, MET pathway activation *via* increased expression of receptor or ligand is frequently implicated in TKI resistance (10–12). Treatment strategies targeting both receptors using a combination of single-agent EGFR and MET inhibitors do not cover the wide range of resistance mechanisms (13, 14), hence the need for novel approaches to overcome resistance and to achieve clinical benefit. Simultaneous engagement of both EGFR and MET, through a bispecific antibody (BsAb), is a potential strategy to overcome resistance and achieve greater efficacy (15).

Identification of an antagonist antibody targeting MET can be challenging as the mechanism of action depends on the valency of the antibody for the tumor target antigen. Such antibodies are referred to as anti-MET, which modulate the activity of c-Met, also called tyrosine-protein kinase Met or hepatocyte growth factor receptor, which is a protein encoded by the *MET* gene. Upon ligand binding, MET dimerizes and initiates signaling pathway activation (16). Therefore, antibodies that induce dimerization of MET may have agonistic activity (17), although antagonistic bivalent MET monoclonal antibodies (mAbs) have been reported (18, 19).

An antibody with a monovalent anti-MET binding arm may prevent MET dimerization-based agonism (20, 21). However, an antibody with this property, such as onartuzumab, did not have a favorable clinical profile (22–24), likely due to (1) inability to induce Fc-mediated effector functions; (2) reduced MET downmodulation *via* internalization by monovalent molecules; and (3) solely targeting MET, which may trigger development of resistance *via* oncogenic EGFR signaling. Thus, we embarked on

‡ Both authors contributed equally.
* For correspondence: Mark L. Chiu, markchiu03@gmail.com.
Present address for G. Mark Anderson: Genome Profiling LLC, Wayne, Pennsylvania, USA.
Present address for Paul W.H.I. Parren: Lava Therapeutics, Utrecht, The Netherlands.
Present address for William R. Strohl: BiStro Biotech Consulting, LLC, Bridgewater, New Jersey, USA.
Present address for Mark L. Chiu: Tavotek Biotherapeutics, Spring House, Pennsylvania, USA.

discovering a molecule with a different molecular format and distinct epitope to improve efficacy.

BsAbs that target EGFR and MET through distinct epitopes and architecture have had varying clinical results (25–28). To maximize inhibition of EGFR and MET pathways, we aimed at discovering a novel BsAb that combines all the previously described mechanisms of action for EGFR and MET antibodies but without inducing receptor dimerization and activation. The BsAb would have two binding arms: one monovalent arm that engages EGFR and the other monovalent arm that engages MET.

To enable the selection of the optimal bispecific molecule, we screened a panel of BsAbs in an empirical approach that led to the selection of amivantamab (JNJ-61186372), an EGFR × MET BsAb that has activity in EGFR TKI-resistant NSCLC models (29). Here, we describe a versatile selection strategy, provide structural insights in the binding of amivantamab, and present novel functional *in vivo* antitumor data.

Results

Parental antibody selection criteria and procedure for generating BsAbs

The controlled Fab-arm exchange (cFAE) platform was used to generate a panel of 40 (5 MET parental mAbs with 8 EGFR parental mAbs) MET × EGFR BsAbs in the DuoBody format (30) (Fig. 1*A*). The BsAb quality was confirmed as being monodisperse by size-exclusion chromatography and purity by SDS-PAGE. The anti-gp120 antibody b12 was included as a nonbinding arm of control BsAbs that had either an EGFR or MET binding arm to generate monovalent control antibodies. The parental antibodies were chosen to cover a broad epitope space for both MET and EGFR mAbs from different cross-block groups, sequence diversity (unique heavy chain complementarity-determining region 3 [CDR-H3] sequence clusters), binding affinity (human–cynomolgus monkey cross-reactivity for EGFR mAbs; human–rhesus monkey cross-reactivity for MET mAbs), and ligand-blocking ability (Table S1).

Since residual parental MET homodimer mAbs can result in an agonistic response, an excess of EGFR homodimer mAb was used in the cFAE reaction to minimize the levels of residual MET homodimer mAbs. The cFAE preparations were analyzed by cation exchange chromatography to confirm the generation of BsAb species and to determine the percentage of residual homodimer in the batches. The homodimer materials were included as reference in the same run. The cation exchange chromatography showed successful generation of a BsAb species was observed after the exchange process when there was a peak located in between the elution peaks of the two-originating parental mAb homodimer peaks. The percentage of residual homodimers are listed in Table S2.

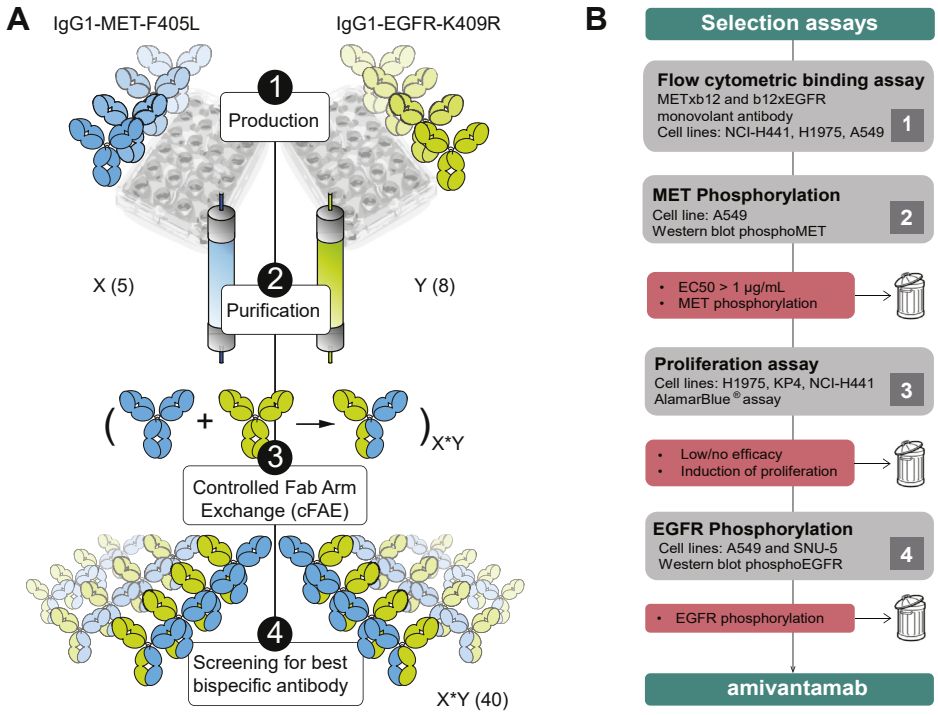

Figure 1. Procedure for generating BsAbs panel and strategy for identification of lead BsAb. *A*, the *blue panel* represents an array of five IgG1 anti-MET and one control anti-gp120 (b12) mAbs with the leucine to phenylalanine substitution at position 405 (F405L). The *green panel* represents an array of eight IgG1 anti-EGFR and one control anti-gp120 mAbs with the lysine to arginine substitution at position 409 (K409R). Upon separate cell-culture growth, each mAb was purified using protein A chromatography. The grid of BsAbs was generated by cFAE for hit selection. *B*, elimination strategy for the identification of optimal lead BsAb. A schematic flowchart that outlines the selection of the lead bivalent EGFR×MET bispecific antibody. The steps include binding of EGFR/MET monovalent BsAbs by flow cytometry to NCI-H441, H1975, and A549 cells; confirmation of the absence of MET phosphorylation in A549 cells; determination of the minimal proliferation in H1975, KP4, and NCI-H441 cells; and absence of cross phosphorylation of EGFR. BsAb, bispecific antibody; EGFR, epidermal growth factor receptor; MET, mesenchymal–epithelial transition factor.

Selection of the lead BsAb

We used an elimination strategy to discard BsAb molecules with unwanted properties at predefined decision points: sufficient monovalent binding affinity (EC_{50} <1 μg/ml, which is within the range of serum concentration of a therapeutic mAb (31)), minimal induction of EGFR and MET phosphorylation, and minimal cell proliferation *via* direct or cross talk activation of EGFR and MET.

Selection phase 1: Binding assay

The first phase of the selection process focused on the binding properties of the antibodies (Fig. 1*B*). A key requirement of the BsAb was the ability to bind both targets in a monovalent format with affinity EC_{50} <1 μg/ml. Molecules with EC_{50} >1 μg/ml were considered low or poor binders and discarded (Fig. 2*A*). Functionally monovalent MET×b12 BsAbs bound well to all cell lines tested, whereas the reactivity of the EGFR panel was more diverse with monovalent EGFR C, EGFR D, EGFR F, and EGFR G BsAbs binding poorly (EC_{50} >1 μg/ml). Binding for monovalent EGFR BsAbs was ranked EGFR H > EGFR E > EGFR B > EGFR A; for monovalent MET BsAbs, binding was ranked MET B > MET A > MET C > MET D > MET E. None of the MET×EGFR BsAb combinations had enhanced binding as compared with their respective monovalent controls (data not shown).

Selection phase 2: MET phosphorylation assay

In A549 cells, MET was not phosphorylated under steady-state conditions in the absence of HGF. An agonistic bivalent antibody MET 5D5 IgG1 and a functionally monovalent bispecific version of MET 5D5 (MET 5D5×b12) were used as positive and negative controls for MET phosphorylation, respectively (Fig. 2*B*; Western blots quantified agonistic

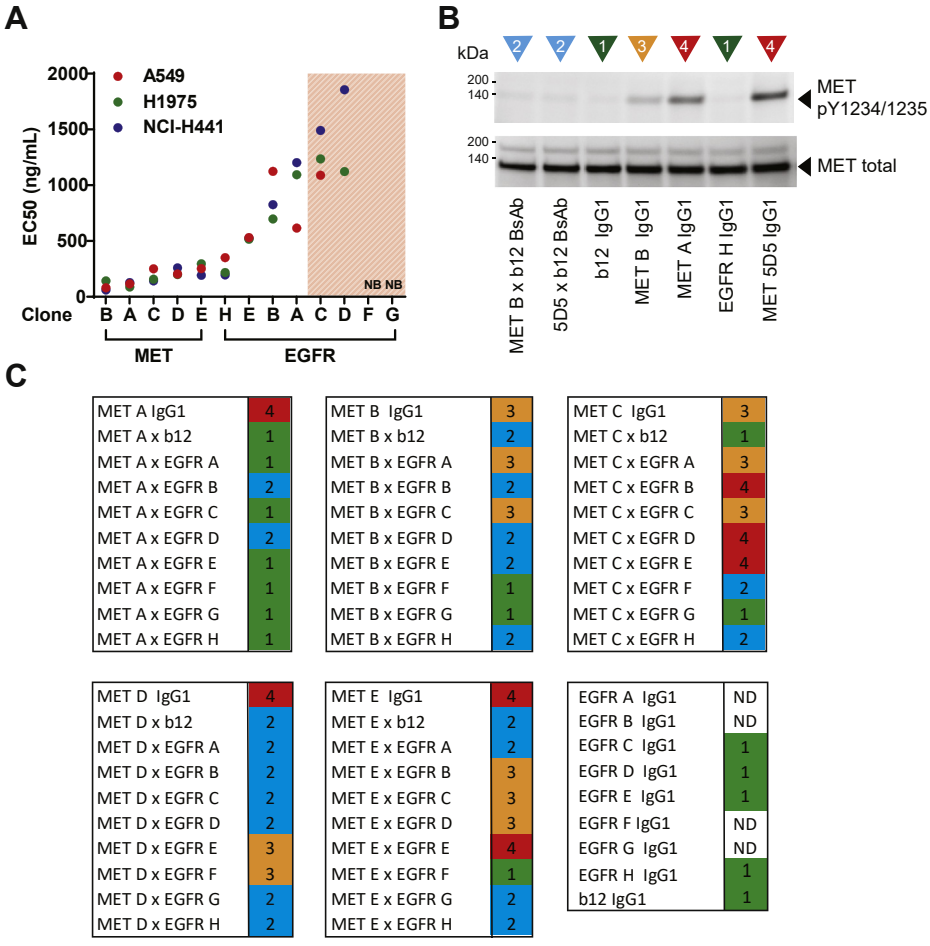

Figure 2. Selection phase 1. *A*, binding activity of functionally monovalent BsAb to NCI-H441, H1975, and A549 cells. Monovalent BsAbs (b12×EGFR and MET×b12) were screened for binding to NCI-H441, H1975, and A549 cell lines. The binding EC_{50} values are shown as *red*, *green*, and *blue dots* for A549, H1975, and H441 cells, respectively. Monovalent EGFR C and EGFR D molecules had EC_{50} values greater than 1 μg/ml (marked by *dotted line*). Monovalent EGFR F and EGFR G BsAbs did not show appreciable binding, indicated as NB. *B*, identification of agonistic EGFR×MET BsAbs *via* MET phosphorylation in A549 cells. MET agonism was measured *via* MET phosphorylation in A549 cells incubated with MET×EGFR BsAbs. Equal amounts of sample on the Western blot were confirmed by the equivalent levels of total MET. The absence (similar to negative control antibody and untreated cell-only control) or low levels of MET phosphorylation levels were shown as *dark green triangles* with a score of 1. Low levels of MET phosphorylation levels (just above the detection limit) were shown as *blue triangles* with a score of 2. Medium levels of MET phosphorylation levels (like MET B IgG1 mAb) were shown as *orange triangles* with a score of 3. High levels of MET phosphorylation levels (like control MET 5D5 IgG1 mAb) were shown as *red triangles* with a score of 4. *C*, overview of MET antagonism score for all assessed BsAb. The same color scheme was used as in *B*. BsAb, bispecific antibody; EGFR, epidermal growth factor receptor; MET, mesenchymal–epithelial transition factor.

activity of antibodies Fig. S1). BsAbs with a score ≥3 and 4 were deselected (Fig. 2*C*).

None of the tested bivalent EGFR parental mAbs induced MET phosphorylation. Although all bivalent MET parental mAbs induced MET phosphorylation, no agonistic activity of the METxb12 BsAb combinations was observed, confirming the hypothesis that MET agonistic antibodies can be converted to antagonistic molecules by using (functionally) monovalent formats (20). Some bispecific MET×EGFR molecules induced MET phosphorylation, suggesting that binding of EGFR and MET on the same cell could result in MET dimerization and activation or phosphorylation of MET in *trans*. BsAbs containing the MET C arm that were identified as MET agonists, as with variants with MET arms B, D, and E with scores of 3 to 4, were excluded from further analysis (Fig. 2*C*). No combinations containing EGFR H were agonistic, even when combined with MET C, which induced medium to high phosphorylation with other EGFR binders. Furthermore,

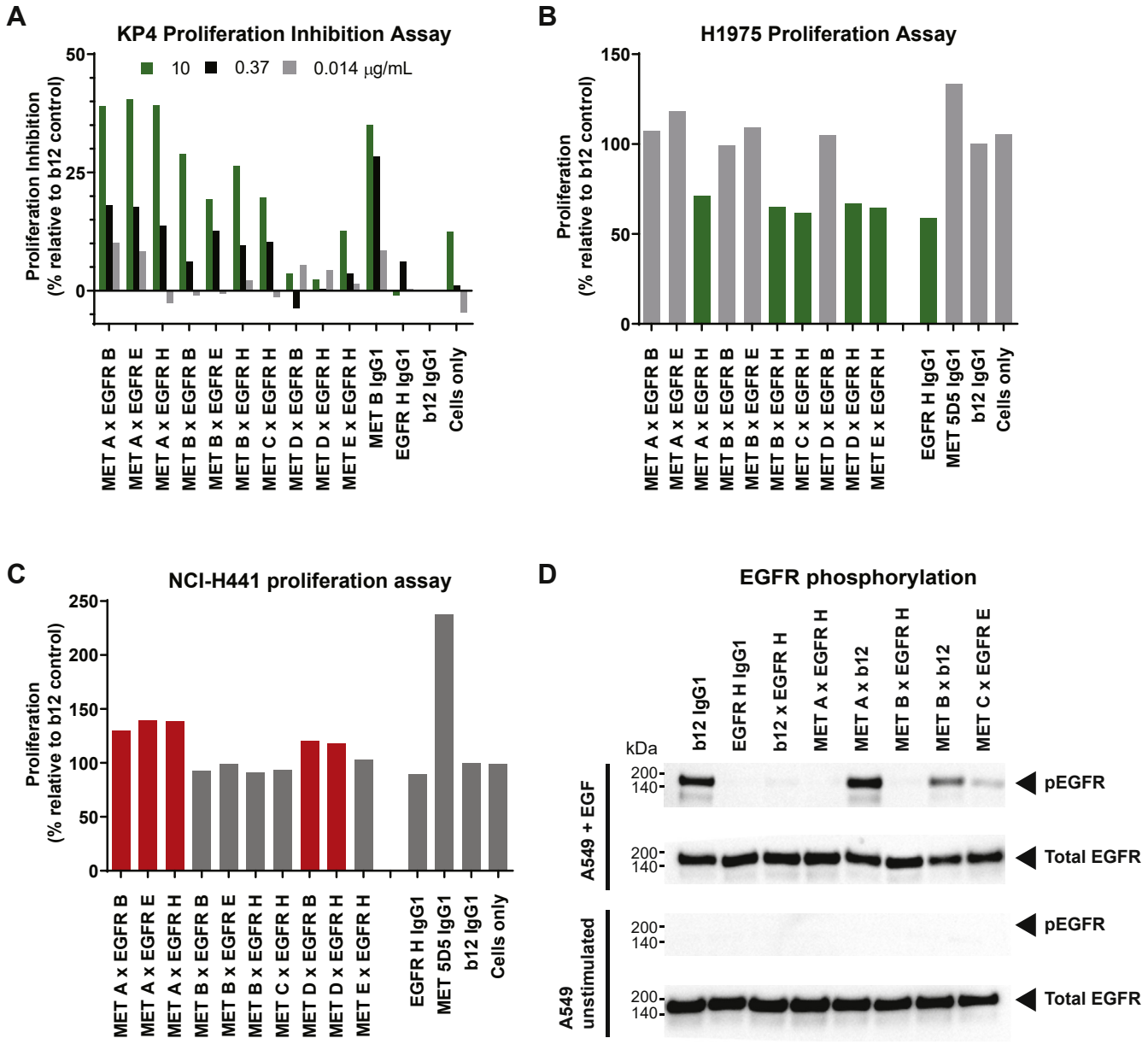

Figure 3. Effect of EGFR×MET BsAbs on cell proliferation. *A*, inhibition of HGF binding-driven proliferation of KP4 cells with an autocrine HGF/MET loop. The bivalent MET B IgG1 mAb served as a positive control. BsAb concentrations of 10 μg/ml (*green*), 0.37 μg/ml (*black*), and 0.014 μg/ml (*gray*) were used. *B*, inhibition of EGF-dependent EGFR based on proliferation of H1975 cells. Bivalent EGFR H IgG1 was used as positive control and b12 IgG1 as negative control. MET 5D5 IgG1 was used as agonistic control mAb. The best proliferation inhibitors that had activity better than the negative control are indicated by *green bars*. *C*, identification of agonistic BsAb-based proliferation of NCI-H441 cells. Same controls as in *B*. BsAbs that induced proliferation are indicated by *red bars*. *D*, EGFR phosphorylation in A549 cells. Unstimulated A549 cells were treated with BsAbs to identify agonistic molecules. None of the BsAbs induced EGFR phosphorylation. In parallel, cells were stimulated with EGF and clear induction of EGFR phosphorylation by EGF was observed, which was effectively blocked by BsAbs containing EGFR arm H and partially by the BsAb with EGFR arm E. Positive control IgG1 EGFR H was fully blocking, and no inhibition was observed with the controls b12 IgG1and monovalent MET A×b12. All samples were loaded to have similar levels of total EGFR (*bottom panels*). BsAb, bispecific antibody; EGF, epidermal growth factor; EGFR, epidermal growth factor receptor; MET, mesenchymal–epithelial transition factor.

molecules containing MET A did not induce MET phosphorylation.

Selection phases 1 and 2 summary

We excluded BsAbs containing the EGFR A, C, D, F, and G arms since they failed the required specifications for affinity and/or induced MET phosphorylation in the A549 phosphorylation assay.

Selection phase 3: Proliferation assays

We examined the impact of receptor phosphorylation *via* proliferation assays of cell lines with differing levels of EGFR and MET. The remaining EGFR×MET BsAb panel was further tested for (1) inhibition of HGF-driven KP4 cell proliferation expressing an autocrine HGF–MET loop and (2) inhibition of H1975 cell proliferation driven by the EGFR signaling pathway.

The percentage of cell proliferation relative to the isotype (negative) control b12 IgG1 in KP4 cells was evaluated at 0.014, 0.37, and 10 μg/ml BsAb concentrations. All BsAbs showed a dose-dependent inhibition of proliferation, except molecules containing the MET D and MET E arms (Fig. 3*A*). This was expected as the parental MET mAbs were unable to block HGF binding to MET *in vitro* (data not shown). Molecules containing the MET A, MET B, and MET C arms had the strongest inhibition of proliferation compared with cells treated with the isotype control.

The percentage of cell proliferation relative to 10 μg/ml b12 IgG1 negative control and bivalent EGFR-H positive control in H1975 cells was evaluated. The bivalent anti-MET 5D5 IgG1 was included as a control agonistic mAb. Except for the positive control and EGFR H BsAb combinations, none of the BsAbs inhibited proliferation of H1975 (Fig. 3*B*).

A third proliferation assay was conducted using NCI-H441 cell lines with equivalent levels of EGFR and MET (Table S3). The NCI-H441 proliferation assay identified agonistic MET×EGFR BsAb. BsAbs MET A×EGFR B, MET A×EGFR E, MET A×EGFR H, MET D×EGFR B and MET D×EGFR H induced mild proliferation of NCI-H441 cells, albeit less pronounced than the agonist MET 5D5 IgG1 control (Fig. 3*C*).

Based on these proliferation assays, we deselected BsAb combinations containing MET A, MET D, and MET E crossed with EGFR B arms. BsAbs with the MET B and C arms in combination with EGFR H were selected for further characterization.

Selection phase 4: EGFR phosphorylation assay

The identified molecules did not induce MET phosphorylation in A549 cells, yet some induced proliferation of NCI-H441 cells (Fig. 3*C*), suggesting that another signaling pathway could be activated due to induction of EGFR phosphorylation *via* cross-linking of MET and EGFR (32–34).

To identify agonistic BsAbs that induced EGFR activation in the absence of EGFR ligand and inhibited ligand-induced EGFR phosphorylation, we lysed cell lines treated with the antibodies and determined EGFR Tyr1068 phosphorylation. In A549 cells, which have low MET and moderate EGFR expression, no EGFR phosphorylation was observed in unstimulated cells. Clear EGFR phosphorylation was observed by treating the cells with EGF and effectively blocked by BsAbs containing EGFR H, partially by BsAb MET C×EGFR E, and not by the MET A×b12 BsAb control (Fig. 3*D*). In contrast to EGFR H, the EGFR E epitope was located outside the EGF binding site and did not block EGF binding to EGFR (not shown).

No EGFR phosphorylation was observed by any of the tested MET×EGFR BsAbs in the absence of EGF, confirming the lack of MET-induced EGFR cross-phosphorylation in A549 cells.

Final selection

Only BsAbs containing the EGFR H arm inhibited H1975 cell proliferation and EGF-induced EGFR phosphorylation in A549 cells. Hence, BsAbs with any other EGFR arm were rejected. BsAbs containing the MET C arm were also discarded as all combinations containing this arm and an EGFR arm with affinity EC_{50} values <1 μg/ml also induced MET phosphorylation (Fig. 2*C*). BsAbs containing the MET D and E arms poorly inhibited KP4 cell proliferation, rendering them unsuitable (Fig. 3*A*). BsAbs containing MET A and D arms were slightly agonistic in the NCI-H441 proliferation assay, although the effect was small compared with the positive control MET 5D5 IgG1 (Fig. 3*C*). Altogether, the MET B×EGFR H BsAb showed the most optimal properties and with growth in a proprietary cell line for production of parental mAbs with low fucose Fc production, the BsAb became amivantamab.

Interactions between amivantamab and MET

The crystal structure of the MET B Fab arm of amivantamab bound to human MET Sema-PSI region was solved to better understand the potent inhibition of MET signaling. The structure of the Fab–Sema-PSI complex was determined to 3.1-Å resolution with one complex in the $P4_32_12$ asymmetric unit (Table S4). The structure contained MET residues 40 to 564 with glycans N-linked to residues N45, N106, N149, N202, and N405, Fab heavy chain residues 1 to 222, and Fab light chain residues 1 to 213. The Fab–Sema-PSI combining site was well defined by the electron density, which allowed reliable positioning of the binding residues.

The amivantamab Fab bound to the MET Sema domain using all CDRs except CDR-H1 (Fig. 4*A*). The Sema domain had a seven-bladed β-propeller with four antiparallel β-strands per blade. The Fab bound to the outside wall of the propeller *via* interactions predominantly with the long loops connecting propeller blades 1 to 2 (loop 1–2; epitope residues D94, F96-D100, and S103-N106) and blades 2 to 3 (loop 2–3; epitope residues F162-P164, I166, and E167). The Fab also had interactions with intra-blade 3 loop C2D3 (epitope residues T222 and D224) and the disulfide-bonded pair (C98-C160) that bridged β-strand D2 with the mid-region of loop 1 to 2. The Fab CDR-H2, -H3, -L2, and -L3 (paratope residues $W50^H$,

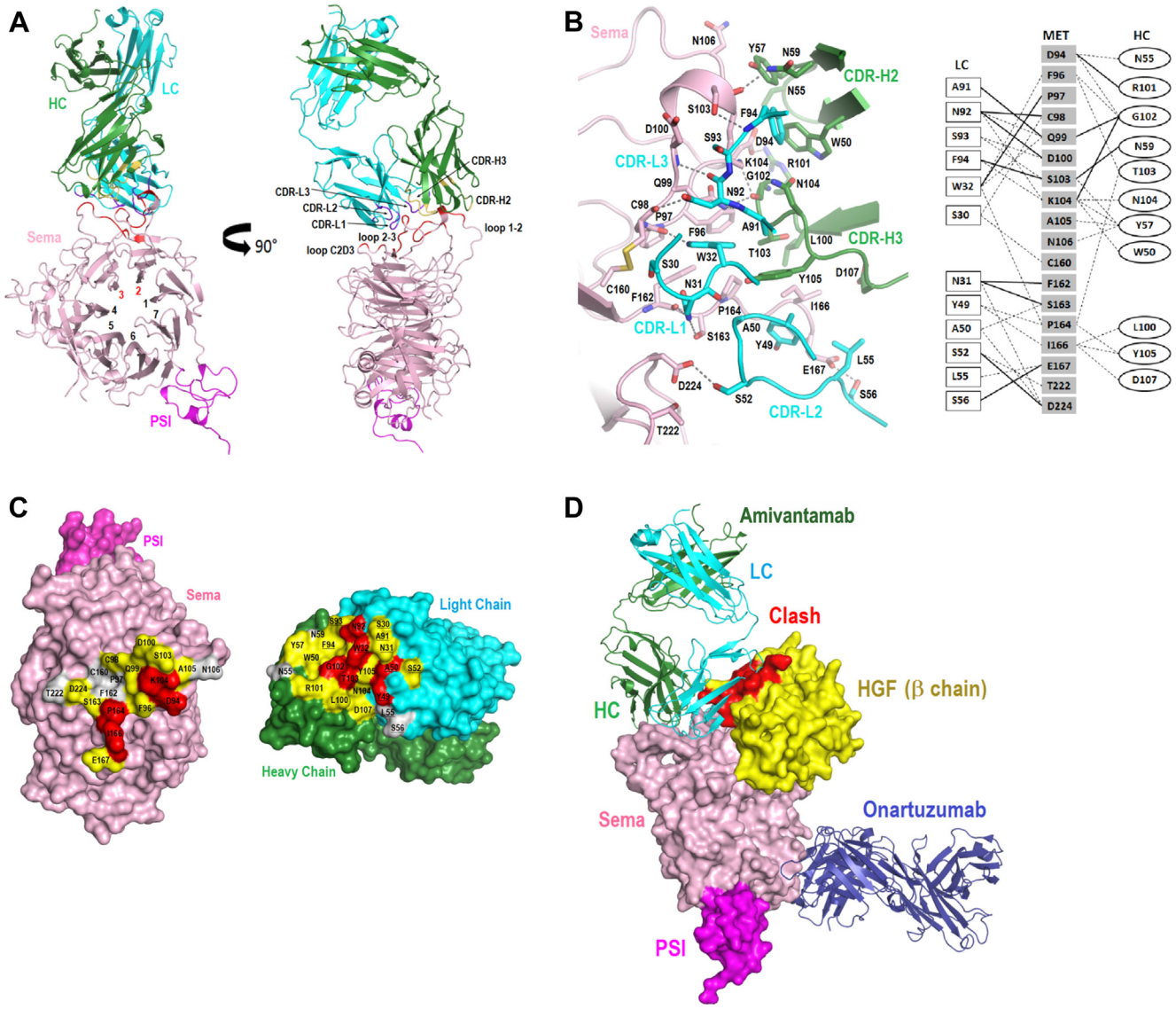

Figure 4. Epitope of anti-MET arm of amivantamab based on the crystal structure of MET Sema-PSI–Fab complex. *A*, representation of the crystal structure. The Fab light (LC, *blue*) and heavy (HC, *green*) chains bound to the Sema domain (*pink*) of MET. The numbers in the center of Sema refer to the seven blades that form Sema β-propeller structure (*red numbers* for Fab-binding blades). The epitope, LC paratope, and HC paratope regions are shown in *red*, *purple*, and *yellow*, respectively. The binding CDRs and MET loops are labeled. *B*, interactions between amivantamab and MET. The *left panel* shows a close view of the combining site with hydrogen bond interactions indicated as *dashed lines*. The *right panel* shows an interaction map with hydrogen bonds as *solid lines*, van der Waals interactions as *dashed lines*, MET, LC and HC residues in *gray boxes*, *white boxes*, and *ovals*, respectively. *C*, open book view of the interface between MET (*left*) and Fab (*right*). Residues at the interface were labeled and colored according to their buried surface area (*red* for residues that bury greater than 75% of their total area, *yellow* for 45%–74% range, and *gray* for 15%–44% range). Light chain residues are *underlined*. *D*, overlay of MET crystal structures bound to either amivantamab or onartuzumab + HGF. The HGF region that clashes (distance between atoms < 1.5 Å) with the LC of amivantamab is shown in *red*. HGF, hepatocyte growth factor; MET, mesenchymal–epithelial transition factor.

$N55^H$, $Y57^H$, $N59^H$, $L100^H$ -$Y105^H$, $D107^H$, $Y49^L$, $A50^L$, $S52^L$, $L55^L$, $S56^L$, and $A91^L$ -$F94^L$) were positioned along the folded mid-section of loop 1 to 2, stabilizing this long loop in a folded down conformation. CDR-L1 (paratope residues S30-W32) interacted exclusively with loops 2 to 3 and C2D3 (Fig. 4, *A* and *B*).

The large 1000 $Å^2$ interface between the Fab and Sema was dominated by polar interactions (Fig. 4*B*). Of the 18 epitope residues, 11 had hydrogen bond interactions with the Fab—the paratope counterpart had 10 of the 23 residues having hydrogen bonds with Sema. The tightly packed interface between the Fab and Sema domains involve hydrogen bond interactions between both protein backbone atoms.

Epitope residues D94, Q99, K104, P164, and I166 of MET were buried into the Sema–Fab combining site and had extensive interactions with the Fab (Fig. 4, *B* and *C*). The side chain of D94 had a hydrogen bond contact with the side chain of R101 (CDR-H3), but these residues could adopt different conformations in solution and form a stronger salt bridge interaction. Q99 and K104 had hydrogen bond contacts with the carbonyl group of G102 (CDR-H3), a glycine strategically located in a crowded region of the combining site (Fig. 4*B*). P164, F96, P97, F162, and P164 constituted the lining of a

shallow cavity on Sema. F96 and F162 formed a cluster of aromatic residues with Fab residues W32 (CDR-L1), Y49 (CDR-L2), and Y105 (CDR-H3). I166 was buried by a portion of this aromatic cluster and the side chain of residues L100, D107 (CDR-H3), and L55 (CDR-L2). Taken together, these paratope–epitope interactions mediated a high level of specificity to amivantamab binding to MET.

Amivantamab Fab binding to MET stabilized the Sema loop 1 to 2 in a conformation slightly different from other MET structures (Protein Data Bank [PDB] codes 1SHY, 4K3J, 2UZX, and 2UZY) (20, 35, 36). The top of loop 1 to 2 was shifted about 6 Å toward amivantamab, which together with smaller shifts of loop 1 to 3 located these binding loops closer to the Fab, optimizing their interactions with the CDRs (Fig. S2). The Sema to PSI orientation was roughly 20° and 30° more open in the amivantamab- and onartuzumab-bound structures, respectively, than in the InlB-bound structures.

Amivantamab antagonized HGF-induced signaling of MET by blocking binding of the β-chain of HGF to the MET Sema domain (Fig. 4*D*). Unlike amivantamab, onartuzumab does not block directly the HGF β-chain from binding to MET (20). Overlay of the MET structures bound to either amivantamab or HGF β-chain and onartuzumab (PDB code 4k3J) (20) demonstrated that the anti-MET light chain of amivantamab had multiple steric clashes with the HGF β-chain (Fig. 4*D*). Specifically, the light chain clashed with HGF residues 498 to 502, 552 to 556, and 619 to 628, which prevented simultaneous binding to MET. The structural overlay indicated that amivantamab would not antagonize the binding of onartuzumab to MET. Amivantamab bound to a patch on the α-chain of Sema away from the region recognized by onartuzumab, which bound to the β-chain of Sema and closer to the PSI domain, and amivantamab Fab binding did not induce conformational changes that impacted the onartuzumab epitope.

Amivantamab EGFR epitope

The amivantamab EGFR H-binding arm is identical to that of zalutumumab. The epitope mapping for the EGFR binding arm was partially presented in a manuscript that was later retracted for unrelated reasons (37). An expanded and verified dataset is presented here. EGFR H binds to a conformational epitope on native EGFR but not to heat-denatured EGFR (Fig. S3*A*), which contrasted with a control polyclonal antibody that recognized both native and denatured EGFR (Fig. S3*B*).

By flow cytometry, the EGFR H bound similarly to both full-length EGFR and EGFRvIII (which lacked EGFR domains I and II)-transfected cells, indicating the EGFR H epitope was within domains III and IV (Fig. S3*C*).

To map the epitope, cross competition of EGFR H was run with mAbs known to bind EGFR domain III and block EGF such as cetuximab, a human–murine chimeric IgG1 containing the Fv of mouse mAb M225 (38). M225-FITC blocked binding of cetuximab, but only blocked EGFR H and M528 at a lower extent (Table S5). EGFR H-FITC blocked binding of cetuximab and less so M528. M528-FITC inhibited cetuximab but EGFR H weakly. Thus, EGFR H showed a cross-blocking profile different than M528, M225, and cetuximab, thereby indicating that these epitopes were not the same.

The EGFR H epitope was further mapped using tissues expressing murine and swine EGFRs, which differ from human EGFR by a few amino acid residues. The binding epitopes of M225 and M528 were located in EGFR AA region 294 to 475; therefore, domain IV (AA 480–620) was excluded from this analysis (39). Fig. S4*A* shows immunohistochemical EGFR H staining of mouse tongue, swine tongue, and human tonsil tissue. Strong positive staining demonstrated EGFR H binding to human tonsil epithelium but not to mouse or swine tongue tissue as compared with human IgG-KLH negative controls showing faint red staining due to nonspecific background staining in swine and mouse tissue. Since EGFR H did not bind to murine and swine EGFR, the epitope was mapped to residues in EGFR domain III that differ from human EGFR (Table S6 and Fig. S4*B*). These 17 residues were used for site-specific EGFR mutagenesis for binding experiments. Figure 5*A* and Fig. S5 show the binding affinity of EGFR H and M225 to the EGFR mutants measured by flow cytometry and the mutation location in the EGFR–transforming growth factor alpha (TGFα) structure. EGFR H completely lost affinity for K465E-EGFR (which disrupts cetuximab binding to EGFR) and had reduced affinity for I467M-EGFR. The K465 mutation resulted in different binding profile between the bivalent mAb formats of EGFRH mAb (no binding) and cetuximab (reduced binding). However, there was no difference in the Fab-binding profile for these molecules. In addition, EGFR H Fab showed a slightly reduced affinity for K443R- and S468N-EGFR, suggesting that, although the residues might not be directly involved in binding, they could have an indirect effect. Thus, K443, K465, I467, and S468 were identified as EGFR epitope residues close to the TGFα-binding site. In contrast, the M225 Fab had reduced affinity for G471A-EGFR. The epitope of EGFR H had some overlap with the cetuximab epitope in EGFR domain III (Fig. 5*B*), whereas EGFR H and cetuximab had overlapping but not similar epitopes. First, EGFR H and cetuximab/M225 had different cross-blocking profiles (Table S5): M528 was blocked more effectively by cetuximab/M225 than by EGFR H. Second, K465E-EGFR showed complete loss of binding to EGFR H, whereas M225 still bound at high mAb concentrations (Fig. S5).

Amivantamab was more effective than EGFR and MET TKIs in an EGFR mutant xenograft model with MET pathway activation

The antitumor activity of amivantamab was compared with small molecule EGFR inhibitor erlotinib and MET inhibitor crizotinib *in vivo*. The HCC827 cell line endogenously expresses high levels of EGFR with an activating mutation (exon 19 deletion) and high levels of MET. We engineered this cell line to overexpress human HGF to provide additional activation of the MET pathway. Amivantamab demonstrated potent antitumor activity in this model, with tumor growth inhibition (TGI) of 99.8% ($p < 0.05$) at day 34, and a durable response that continued 8 weeks post dosing cessation. No activity was

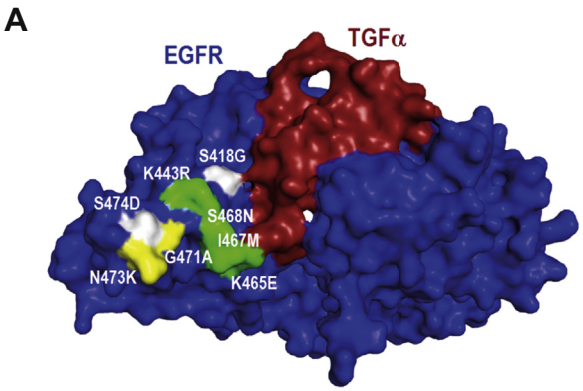

Substitution	EGFR H	M225
K465E	↓↓↓↓	↓↓↓
I467M	↓↓↓	↓↓
N473K	similar	↓
S474D	similar	similar
K443R	↓	↓
S468N	↓	↓↓
G471A	similar	↓
S418G	similar	similar

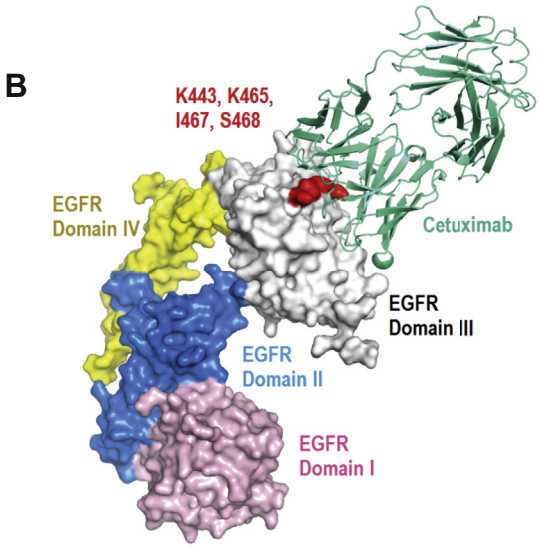

Figure 5. Epitope mapping of the anti-EGFR arm of amivantamab. *A*, differences in affinity of EGFR H (amivantamab arm) and M225 (mAb containing cetuximab Fv) to single-point mutants of EGFR in reference to wildtype EGFR. The *right panel* shows the location of the mutations in the crystal structure of EGFR bound to ligand TGFα (PDB code 1MOX; reference (48)). TGFα (*brown*) is shown at its binding pocket on EGFR domain III (*blue*). Mutations S418G and S474D (*white regions*) do not impact EGFR H and M225. Mutations K465E, I467M, K443R, and S468N (*green regions*) impact both EGFR H and M225, although with different strengths. Mutations G471A and N743K (*yellow regions*) impact only M225. *B*, possible partial epitope (residues K443, K465, I467, and S468; shown in *red*) of the anti-EGFR arm of amivantamab mapped on the crystal structure of EGFR bound to cetuximab (Protein Data Bank 1YY9, (48)). EGFR domains and cetuximab are indicated. EGFR, epidermal growth factor receptor; TGFα, transforming growth factor alpha.

observed with crizotinib as monotherapy, suggesting that blocking MET alone was not sufficient to inhibit tumor growth in this model (Fig. 6). Erlotinib as monotherapy and the combination of erlotinib and crizotinib showed statistically significant reductions in tumor growth at day 34 compared with the controls with TGI values of 61% and 81%, both $p < 0.05$. The TGI with the combination of small molecule inhibitors was also significant ($p < 0.05$) compared with erlotinib alone. Overall, amivantamab demonstrated a more effective antitumor response compared with the combination of EGFR and MET small molecule inhibitors in this EGFR mutant xenograft model with MET pathway activation.

Discussion

The DuoBody cFAE platform is a versatile postproduction exchange process that enables the generation of large BsAbs libraries and selection of the lead bispecific molecules in an unbiased and empirical approach, concomitantly in the final format based on functional data (40). A panel of BsAbs targeting EGFR and MET was generated and screened in a series of assays to select an optimal BsAb with the potential to inhibit EGFR and MET pathways. Typically, the process of BsAb selection utilizing parental mAbs with highest affinity can result in isolating BsAbs with unwanted properties that would not have been predicted based on individual properties.

Candidates were first screened for their monovalent binding affinity to EGFR and MET in cell lines and subsequently screened for their ability to inhibit MET phosphorylation. Proliferation assays in H1975, KP4, and NCI-H441 cells helped to identify candidates that could inhibit EGFR- and MET-dependent cell growth and deselect combinations that induced proliferation. Identified leads were further tested for potential cross-phosphorylation of EGFR by MET in the absence of ligand in A549 cells. The effect of EGF could be fully neutralized by all the lead molecules containing EGFR H

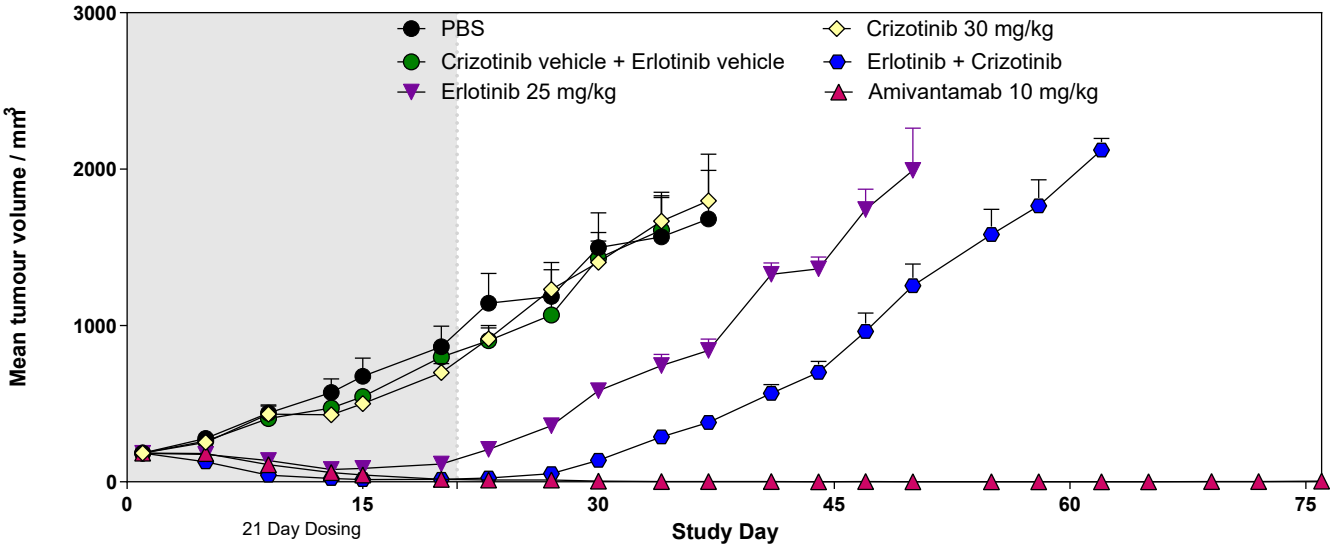

Figure 6. Amivantamab showed superior efficacy in the HCC827-HGF model. Animals (groups of nine) were treated with agents listed above for the first 21 days of study. Subcutaneous tumors were measured twice weekly and the results plotted as the mean tumor volume, expressed in mm^3 + standard error of the mean (SEM), of each group. The plots are labeled PBS control as *black circles*, crizotinib vehicle and erlotinib vehicle as *green circles*, 25 mg/kg erlotinib as *purple triangles*, 30 mg/kg crizotinib as *white rhombi*, 25 mg/kg erlotinib and 30 mg/kg crizotinib as *blue circles*, and 10 mg/kg amivantamab as *red triangles*.

and partially by MET C×EGFR E BsAb, indicating that the EGF blocking capacity of EGFR H was retained in the bispecific molecules. We hypothesized that the MET A×EGFR BsAbs may be able to induce EGFR phosphorylation, explaining the unexpected agonistic activity in the NCI-H441 proliferation assay. The NCI-H441 cells were considered unsuitable for these assays given their heterozygous KRAS status and high constitutive EGFR phosphorylation. In A549 cells, no EGFR phosphorylation was observed with MET A×EGFR H or MET C×EGFR E molecules, but we could not preclude that this could be a result of lower overall MET expression. As an alternative, we also assessed EGFR phosphorylation by BsAbs MET A×EGFR H and MET C×EGFR E in MET overexpressing SNU-5 cells (data not shown). Under steady state conditions where EGFR was constitutively phosphorylated, BsAb MET A×EGFR H increased this phosphorylation. Addition of EGF also increased EGFR phosphorylation, which was inhibited by bivalent and monovalent versions of antibody EGFR H but not by BsAbs MET A×EGFR H and MET C×EGFR E. This suggested that, with increasing surface expression of MET, MET-EGFR cross-phosphorylation induced by certain MET×EGFR BsAbs targeting specific epitopes would increase. Based on these results, BsAbs MET A×EGFR H and MET C×EGFR E were discarded and BsAb MET B×EGFR H was selected as the lead bispecific candidate for its superior properties. The BsAb MET B×EGFR H was then generated in cell lines to have a low fucose Fc form to enhance antibody-dependent cellular cytotoxicity (ADCC) activity resulting in the drug molecule named amivantamab (41).

The *in vitro* potency and action of the selected lead candidate were verified in relevant *in vivo* models. Amivantamab treatment showed superior efficacy in the HCC827-HGF model compared with small molecule inhibitors of EGFR and MET, consistent with previous studies (29). Inhibition of the cell proliferation *in vitro* did not reflect all mechanisms of action that may be involved *in vivo*. The lead bispecific molecule has multiple mechanisms including ADCC, receptor downmodulation, and trogocytosis (29, 42, 43).

The crystal structure of the anti-MET Fab arm of amivantamab bound to human MET Sema-PSI provided further insight on the structural and functional basis of MET antagonism by amivantamab. The amivantamab Fab bound to the MET Sema domain using all CDRs except CDR-H1, and the large interface between amivantamab and MET was dominated by polar interactions. Key epitope residues D94, Q99, K104, P164, and I166 were buried into the Sema–Fab interface, had critical interactions with the CDRs, and elucidated a high level of amivantamab specificity toward MET. In comparing this crystal structure to the HGF + onartuzumab (PDB code 4k3J (20)), there was extensive steric hindrance between the amivantamab anti-MET light chain and the HGF β-chain, which can effectively prevent their simultaneous binding to MET and cause inhibition of HGF-induced MET signaling. The location of the amivantamab epitope on Sema is distinct from that of onartuzumab, which was reported to bind closer to the PSI domain and block the α-chain of HGF (20).

Competition studies indicated that the binding site of the α-chain of HGF (NK1 region) lay within the β-chain of the Sema domain (residues 308–514) and overlapped partially with the binding site of onartuzumab (20) and InlB IR region (44). These data confirmed previous observations that both parental antibody MET B and amivantamab were able to effectively block binding of HGF to recombinant MET (29). Because amivantamab and onartuzumab bound to opposite sides of Sema, it was unlikely that amivantamab would clash with the NK1 region of HGF and directly block the interaction of the α-chain of HGF with Sema. A three-dimensional structure of MET bound to the α-chain of HGF would be needed to

facilitate a clearer understanding of MET and HGF interactions and a more complete vision about the antagonist phenotypes of amivantamab and onartuzumab.

Amivantamab effectively inhibited EGFR ligand binding (29), indicating that its epitope on EGFR was near the ligand-binding site. The amivantamab epitope was mapped to EGFR domain III and essential EGFR residues (K465, I467, K443, and S468). Although this partial epitope overlaps with the cetuximab epitope, the EGFR H arm of amivantamab could not bind the EGFR mutant K465E, in contrast to the murine variant of cetuximab sharing the variable domains with cetuximab. Furthermore, mAb M528 (another anti-EGFR antibody) blocked cetuximab but not amivantamab binding to EGFR. These findings indicate that amivantamab and cetuximab recognize overlapping yet different epitopes on EGFR domain III (38). Cetuximab partially occludes the ligand-binding site and sterically prevents the receptor from adopting an extended conformation required for dimerization. We hypothesize that amivantamab binding had a similar effect on EGFR (38, 45).

BsAbs are entering clinical evaluation in significant numbers, with some exciting successes. However, the complexities of choosing the best parental antibody based on affinity, epitope, and functional activity are multiplied when developing BsAbs. In many instances, the obligate activity of the bispecific Ab cannot be predicted from current knowledge of the parental antibody properties (40), especially since the parental MET mAbs were all agonistic. Success requires starting with a broad set of target mAbs, executing a screening approach focused on the critical functional attributes of the desired BsAb.

Amivantamab is under clinical development for the treatment of NSCLC (NCT02609776, NCT04077463) and has shown preliminary activity in diverse EGFR-mutated NSCLCs and MET-driven disease (46). Based on its unique mode of action, which includes induction of trogocytosis from macrophages, ADCC from natural killer cells, and receptor–antibody complex internalization and lysosomal degradation (29, 42, 43), amivantamab may provide significant benefit to patients with NSCLC and other malignancies associated with aberrant EGFR and MET signaling.

Experimental procedures

Preparation of BsAb panel

The generation of parental antibodies followed expression and purification protocols as described (30, 40). The MET parental mAbs had the F405L mutation and the EGFR parental mAbs had the K409R mutation. The IgG1 b12 arm served as isotype control and null arm to preserve the BsAb architecture. The low fucose parental mAbs were generated using proprietary cell lines. The quality of the BsAb were confirmed as being monodisperse and monomeric *via* size exclusion chromatography and being pure *via* SDS-PAGE.

Flow cytometric binding assay

Binding to cells expressing EGFR and MET (A549 [ATCC CCL-185], NCI-H1975 [ATCC, CRL-5908], and NCI-H441 [ATCC HTB-174] cells) was evaluated using flow cytometry (fluorescence-activated cell sorting [FACS]). All BsAbs and controls were diluted in FACS buffer (PBS supplemented with 1% bovine serum albumin and 0.2% sodium azide). After 1 h incubation, unbound antibodies were removed by a FACS buffer wash. The cells were then incubated with goat anti-human IgG-PE (Jackson) for FACS detection (BD FACS Canto). The mean fluorescence intensity of the cells in the live gate was plotted against antibody concentration, and the EC_{50} was determined by nonlinear regression fitting. Anti-EGFR zalutumumab and anti-MET 5D5 (onartuzumab) were positive controls and anti-CD20 7D8 (Genmab) was the negative control.

MET phosphorylation assay

A549 cells were incubated with 30 μg/ml of test antibody for 15 min and tested for MET phosphorylation using rabbit anti-phospho MET (Tyr1234–1235) (Cell Signaling 3129) and total MET protein using mouse anti-human MET antibody (Cell Signaling 3127). A score of 1 to 4 was given, where 1 = no visible band, 2 = slightly visible band, 3 = phosphorylation comparable with weak agonist (MET B IgG1), and 4 = phosphorylation level similar to positive controls (MET A and MET 5D5 IgG1 mAbs).

Proliferation assays

Test molecules were added to H1975, KP4 (Riken Cell bank, RCB1005), or NCI-H441 cells plated at 5000 or 10,000 (KP4) cells/well in 96-well plates. After 6 (KP4) or 7 (H1975 and NCI-H441) days of incubation at 37 °C and 5% CO_2, the number of viable cells was determined using an AlamarBlue assay (Biosource DAL1100). A_{615} values were measured and plotted in a bar diagram.

EGFR phosphorylation assay

Approximately 10^6 A549 or SNU-5 cells/well were grown overnight in six-well plates and incubated for 15 min with 30 μg/ml of antibody in the absence or presence of 40 ng/ml EGF. After cell lysis, Western blots determined EGFR phosphorylation status with phospho-EGFR (Tyr1068) antibody (Cell Signaling 2234) and total EGFR protein using an anti-EGFR antibody (Cell Signaling 2232).

Expression and purification of proteins for crystallization

Human MET Sema-PSI region (residues 39–564) containing a C-terminal 8xHis tag was expressed in *Tni* PRO insect cells infected with recombinant baculovirus. The culture was harvested 72 h post infection, and the MET Sema-PSI protein was purified by affinity and size exclusion chromatography. Briefly, MET was captured with a Ni-NTA resin (Novagen) equilibrated in TBS, 10 mM imidazole, pH 7.4 and eluted from the column with 250 mM imidazole, TBS, pH 7.4. Fractions containing MET were identified by SDS-PAGE and loaded into a Superdex 200 column (GE Healthcare) equilibrated in 20 mM Tris, 50 mM NaCl, pH 7. The final protein concentration was determined by absorbance at 280 nm.

The anti-MET Fab of amivantamab was transiently expressed in Expi293F cells. Briefly, the cells were cotransfected with separate plasmids encoding the Fab heavy and light chains at 3:1 (light:heavy chain) molar ratio following transfection kit instructions (Life Technologies). The culture was harvested 5 days post transfection, and the Fab was purified by affinity and cation exchange chromatography. Briefly, the Fab was captured with a HiTrap resin (GE Healthcare) equilibrated in PBS pH 7.2 and eluted from the column with a gradient of 30 to 300 mM imidazole in PBS pH 7.2. The eluate was buffer exchanged into 25 mM NaCl, 20 mM MES pH 6.0, bound to a Source 15S column (GE Healthcare), and eluted with a NaCl gradient in 20 mM MES pH 6.0.

Crystallization and structure determination

The amivantamab anti-MET Fab–MET Sema-PSI complex was prepared by overnight mixing of MET and Fab at a molar ratio of 1:1.3 (excess Fab) at 4 °C, while buffer exchanging to 20 mM Hepes pH 7.0. The complex was captured with a monoS 5/50 column (GE Healthcare) equilibrated in 20 mM Hepes pH 7.0 and eluted from the column with a gradient of NaCl. The complex was concentrated to 4.8 mg/ml.

Crystallization trials for the Fab–MET complex were carried out with a Mosquito LCP robot (TTP LabTech) for the setup of sitting drops on 96-well plates (Corning 3550) and a Rock Imager 54 (Formulatrix) for plate storage at 20 °C and automated imaging of drops. Small crystals were initially obtained from 2 M $NH_4(SO_4)_2$, 0.1 M MES pH 6.5, and they were used as seeds in next rounds of optimization. Crystals suitable for X-ray diffraction were obtained from 2.5 M sodium formate, 5% PEG 400 Da, 0.1 M Tris pH 8.5 after multiple rounds of seeding. The crystals were soaked for a few seconds in a cryoprotectant solution containing mother liquor supplemented with 20% glycerol and then flash frozen in liquid nitrogen. X-ray diffraction data were collected with a Pilatus 6M detector on beamline 17-ID at the Advanced Photon Source (Argonne National Laboratory), and the diffraction data were processed with the program HKL2000. The crystal structure of the Fab–MET complex was solved by molecular replacement with PHASER using previously solved MET Sema-PSI (PDB code 1SHY) and anti-HER3 Fab RG7116 (PDB code 4LEO) structures as search models. The structure was refined with PHENIX, and model adjustments were performed using COOT. His tags (at C-terminal of heavy chain and PSI), Fab interchain disulfide bond, heavy chain residues 133 to 139, Sema residues 303 to 309, 407, and glycan linked to N399 are disordered and not included in the structure. The Fab was numbered sequentially and Sema-PSI numbering starts at the N terminus of the signal peptide.

Epitope and paratope residues were assigned within a 4-Å contact distance cutoff using the CCP4 program CONTACT. The epitope area was calculated with the CCP4 program AREA. The buried surface area of binding residues was calculated with the program MOE (47). Structural overlays of equivalent Cα atoms in the Sema domain (residues 40–515; PDB codes 1SHY, 4K3J, 2UZX, and 2UZY) were performed with COOT. Molecular graphics were generated with PyMol (PyMOL Molecular Graphics System, Version 1.4.1, Schrödinger, LLC) and MOE. The atomic coordinates and structure factors for the amivantamab anti-MET Fab–MET Sema-PSI complex were deposited in the RCSB PDB (accession code 6WVZ).

HCC827-HGF xenograft model

Female SCID Beige mice CB17.B6-Prkdc^{scid} Lyst^{bg}/Crl (Charles River) bearing established subcutaneous HCC827-HGF tumors were randomized 13 days post inoculation (day 1). Individual tumor volumes ranged from 144 to 221 mm^3; mean tumor volume ranged from 180 to 184 mm^3. PBS and amivantamab (10 mg/kg) were dosed i.p. biweekly for 3 weeks. Crizotinib (30 mg/kg), erlotinib (25 mg/kg), crizotinib (30 mg/kg) and erlotinib (25 mg/kg), and vehicle controls (0.5% carboxymethyl cellulose in sterile water and 1% carboxymethyl cellulose in 0.1% Tween 80) were dosed daily p.o. for 3 weeks. Subcutaneous tumors were measured twice weekly as the mean tumor volume (mm^3 ± standard error of the mean [SEM]). To calculate the percent tumor growth inhibition (% TGI) for group A *versus* group B, the tumor volumes were log transformed, where A = treated and B = control. The difference between these transformed values was taken at day 1 *versus* the designated day. Means were taken and converted by anti-log to numerical scale. Percentage TGIs were then calculated as (1 – A/B) × 100%. *In vivo* experiment was reviewed and approved by the Charles River Laboratories Institutional Animal Care and Use Committee and was done in accordance with the Guide for Care and Use of Laboratory Animals.

Data availability

All data are contained within the article. Further information and requests of materials used in this research should be directed to Mark Chiu (markchiu03@gmail.com).

Supporting information—This article contains supporting information.

Acknowledgments—The authors thank Bart de Goeij and Wendy Janssen for technical support with *in vitro* assays, Matthias Peipp and Tanja Schneider-Merck for supporting the work on EGFR epitope, and Kristin Strumane and Jeroen Lammerts van Bueren for discussion. We thank Barry Springer and Omid Vafa for their fruitful discussions on the project strategy. Writing assistance was provided by Ramji Narayanan, M. Pharm., CMPP (SIRO Clinpharm Pvt Ltd) funded by Janssen Global Services, LLC, and Gijs Zom (Genmab). Additional editorial support for this article was provided by Tracy Cao, PhD, CMPP (Janssen Global Services, LLC).

Author contributions—J. S., R. M. F. C., W. R. S., J. N., T. V., S. L. M., and M. L. C. designed the research; M. L. C., J. N., S. L. M., J. W., K. M. W., L. W., and R. M. F. C. performed the research; M. L. C., S. L. M., J. S., G. M. A., W. R. S., and P. W. H. I. P. provided

supervision; J. N., R. M. F. C., K. M. C., L. W., and T. V. curated the data; M. L. C., J. N., R. M. F. C., S. L. M., K. M. C., and L. W. analyzed the data; all authors reviewed and edited the manuscript, and approved the final version of the manuscript.

Funding and additional information—The study was funded by Janssen Research and Development, LLC.

Conflict of interest—Joost Neijssen, Luus Wiegman, and Janine Schuurman are employees of Genmab. Paul Parren was an employee of Genmab when this work was completed. Rosa M.F. Cardoso, Kristen Chevalier, and Sheri Moores are employees of Janssen Research & Development. Mark Chiu, Mark Anderson, and William Strohl were employees of Janssen Research & Development when this work was completed.

Abbreviations—The abbreviations used are: ADCC, antibody-dependent cellular cytotoxicity; BsAb, bispecific antibody; cFAE, controlled Fab-arm exchange; EGFR, epidermal growth factor receptor; FACS, fluorescence-activated cell sorting; HGF, hepatocyte growth factor; mAb, monoclonal antibody; MET, mesenchymal–epithelial transition factor; NSCLC, non–small cell lung cancer; PDB, Protein Data Bank; TGFα, transforming growth factor alpha; TGI, tumor growth inhibition; TKI, tyrosine kinase inhibitor.

References

1. Birchmeier, C., Birchmeier, W., Gherardi, E., and Vande Woude, G. F. (2003) Met, metastasis, motility and more. *Nat. Rev. Mol. Cell Biol.* **4**, 915–925
2. Liu, X., Yao, W., Newton, R. C., and Scherle, P. A. (2008) Targeting the c-MET signaling pathway for cancer therapy. *Expert Opin. Investig. Drugs* **17**, 997–1011
3. Bean, J., Brennan, C., Shih, J. Y., Riely, G., Viale, A., Wang, L., Chitale, D., Motoi, N., Szoke, J., Broderick, S., Balak, M., Chang, W. C., Yu, C. J., Gazdar, A., Pass, H., *et al.* (2007) MET amplification occurs with or without T790M mutations in EGFR mutant lung tumors with acquired resistance to gefitinib or erlotinib. *Proc. Natl. Acad. Sci. U. S. A.* **104**, 20932–20937
4. Dulak, A. M., Gubish, C. T., Stabile, L. P., Henry, C., and Siegfried, J. M. (2011) HGF-independent potentiation of EGFR action by c-Met. *Oncogene* **30**, 3625–3635
5. Arrieta, O., Cardona, A. F., Martin, C., Mas-Lopez, L., Corrales-Rodriguez, L., Bramuglia, G., Castillo-Fernandez, O., Meyerson, M., Amieva-Rivera, E., Campos-Parra, A. D., Carranza, H., Gomez de la Torre, J. C., Powazniak, Y., Aldaco-Sarvide, F., Vargas, C., *et al.* (2015) Updated frequency of EGFR and KRAS mutations in NonSmall-cell lung cancer in Latin America: The Latin-American Consortium for the investigation of lung cancer (CLICaP). *J. Thorac. Oncol.* **10**, 838–843
6. Sequist, L. V., Yang, J. C., Yamamoto, N., O'Byrne, K., Hirsh, V., Mok, T., Geater, S. L., Orlov, S., Tsai, C. M., Boyer, M., Su, W. C., Bennouna, J., Kato, T., Gorbunova, V., Lee, K. H., *et al.* (2013) Phase III study of afatinib or cisplatin plus pemetrexed in patients with metastatic lung adenocarcinoma with EGFR mutations. *J. Clin. Oncol.* **31**, 3327–3334
7. Soria, J. C., Ohe, Y., Vansteenkiste, J., Reungwetwattana, T., Chewaskulyong, B., Lee, K. H., Dechaphunkul, A., Imamura, F., Nogami, N., Kurata, T., Okamoto, I., Zhou, C., Cho, B. C., Cheng, Y., Cho, E. K., *et al.* (2018) Osimertinib in untreated EGFR-mutated advanced non-small-cell lung cancer. *N. Engl. J. Med.* **378**, 113–125
8. Yu, H. A., Arcila, M. E., Rekhtman, N., Sima, C. S., Zakowski, M. F., Pao, W., Kris, M. G., Miller, V. A., Ladanyi, M., and Riely, G. J. (2013) Analysis of tumor specimens at the time of acquired resistance to EGFR-TKI therapy in 155 patients with EGFR-mutant lung cancers. *Clin. Cancer Res.* **19**, 2240–2247
9. Oxnard, G. R., Hu, Y., Mileham, K. F., Husain, H., Costa, D. B., Tracy, P., Feeney, N., Sholl, L. M., Dahlberg, S. E., Redig, A. J., Kwiatkowski, D. J., Rabin, M. S., Paweletz, C. P., Thress, K. S., and Janne, P. A. (2018) Assessment of resistance mechanisms and clinical implications in patients with EGFR T790M-positive lung cancer and acquired resistance to osimertinib. *JAMA Oncol.* **4**, 1527–1534
10. Turke, A. B., Zejnullahu, K., Wu, Y.-L., Song, Y., Dias-Santagata, D., Lifshits, E., Toschi, L., Rogers, A., Mok, T., Sequist, L., Lindeman, N. I., Murphy, C., Akhavanfard, S., Yeap, B. Y., Xiao, Y., *et al.* (2010) Preexistence and clonal selection of MET amplification in EGFR mutant NSCLC. *Cancer Cell* **17**, 77–88
11. Engelman, J. A., Zejnullahu, K., Mitsudomi, T., Song, Y., Hyland, C., Park, J. O., Lindeman, N., Gale, C. M., Zhao, X., Christensen, J., Kosaka, T., Holmes, A. J., Rogers, A. M., Cappuzzo, F., Mok, T., *et al.* (2007) MET amplification leads to gefitinib resistance in lung cancer by activating ERBB3 signaling. *Science* **316**, 1039–1043
12. Yano, S., Yamada, T., Takeuchi, S., Tachibana, K., Minami, Y., Yatabe, Y., Mitsudomi, T., Tanaka, H., Kimura, T., Kudoh, S., Nokihara, H., Ohe, Y., Yokota, J., Uramoto, H., Yasumoto, K., *et al.* (2011) Hepatocyte growth factor expression in EGFR mutant lung cancer with intrinsic and acquired resistance to tyrosine kinase inhibitors in a Japanese cohort. *J. Thorac. Oncol.* **6**, 2011–2017
13. Scagliotti, G. V., Moro-Sibilot, D., Kollmeier, J., Favaretto, A. G., Cho, E. K., Grosch, H., Kimmich, M., Girard, N., Tsai, C.-M., Hsia, T.-C., Brighenti, M., Schumann, C., Wang, X. A., Wijayawardana, S. R., Gruver, A. M., *et al.* (2017) A randomized, controlled, open label phase II study of erlotinib (E) with or without the MET antibody emibetuzumab (Emi) as first-line treatment for EGFRmt non-small cell lung cancer (NSCLC) patients who have disease control after an 8-week lead-in treatment with erlotinib. *J. Clin. Oncol.* **35**, 9019
14. Scagliotti, G. V., Shuster, D., Orlov, S., von Pawel, J., Shepherd, F. A., Ross, J. S., Wang, Q., Schwartz, B., and Akerley, W. (2018) Tivantinib in combination with erlotinib versus erlotinib alone for EGFR-mutant NSCLC: An exploratory analysis of the phase 3 MARQUEE study. *J. Thorac. Oncol.* **13**, 849–854
15. Puri, N., and Salgia, R. (2008) Synergism of EGFR and c-Met pathways, cross-talk and inhibition, in non-small cell lung cancer. *J. Carcinog.* **7**, 9
16. Luraghi, P., Schelter, F., Kruger, A., and Boccaccio, C. (2012) The MET oncogene as a therapeutical target in cancer invasive growth. *Front. Pharmacol.* **3**, 164
17. Husain, B., and Ellerman, D. (2018) Expanding the boundaries of biotherapeutics with bispecific antibodies. *BioDrugs* **32**, 441–464
18. Liu, L., Zeng, W., Wortinger, M. A., Yan, S. B., Cornwell, P., Peek, V. L., Stephens, J. R., Tetreault, J. W., Xia, J., Manro, J. R., Credille, K. M., Ballard, D. W., Brown-Augsburger, P., Wacheck, V., Chow, C. K., *et al.* (2014) LY2875358, a neutralizing and internalizing anti-MET bivalent antibody, inhibits HGF-dependent and HGF-independent MET activation and tumor growth. *Clin. Cancer Res.* **20**, 6059–6070
19. Gonzalez, A., Broussas, M., Beau-Larvor, C., Haeuw, J. F., Boute, N., Robert, A., Champion, T., Beck, A., Bailly, C., Corvaia, N., and Goetsch, L. (2016) A novel antagonist anti-cMet antibody with antitumor activities targeting both ligand-dependent and ligand-independent c-Met receptors. *Int. J. Cancer* **139**, 1851–1863
20. Merchant, M., Ma, X., Maun, H. R., Zheng, Z., Peng, J., Romero, M., Huang, A., Yang, N. Y., Nishimura, M., Greve, J., Santell, L., Zhang, Y. W., Su, Y., Kaufman, D. W., Billeci, K. L., *et al.* (2013) Monovalent antibody design and mechanism of action of onartuzumab, a MET antagonist with anti-tumor activity as a therapeutic agent. *Proc. Natl. Acad. Sci. U. S. A.* **110**, E2987–E2996
21. Xiang, H., Bender, B. C., Reyes, A. E., 2nd, Merchant, M., Jumbe, N. L., Romero, M., Davancaze, T., Nijem, I., Mai, E., Young, J., Peterson, A., and Damico-Beyer, L. A. (2013) Onartuzumab (MetMAb): Using nonclinical pharmacokinetic and concentration-effect data to support clinical development. *Clin. Cancer Res.* **19**, 5068–5078
22. Surati, M., Patel, P., Peterson, A., and Salgia, R. (2011) Role of MetMAb (OA-5D5) in c-MET active lung malignancies. *Expert Opin. Biol. Ther.* **11**, 1655–1662
23. Spigel, D. R., Edelman, M. J., O'Byrne, K., Paz-Ares, L., Mocci, S., Phan, S., Shames, D. S., Smith, D., Yu, W., Paton, V. E., and Mok, T. (2017) Results from the phase III randomized trial of onartuzumab plus erlotinib versus

erlotinib in previously treated stage IIIB or IV non-small-cell lung cancer: METLung. *J. Clin. Oncol.* **35**, 412–420
24. Spigel, D. R., Ervin, T. J., Ramlau, R. A., Daniel, D. B., Goldschmidt, J. H., Jr., Blumenschein, G. R., Jr., Krzakowski, M. J., Robinet, G., Godbert, B., Barlesi, F., Govindan, R., Patel, T., Orlov, S. V., Wertheim, M. S., Yu, W., *et al.* (2013) Randomized phase II trial of onartuzumab in combination with erlotinib in patients with advanced non-small-cell lung cancer. *J. Clin. Oncol.* **31**, 4105–4114
25. Lee, B. S., Kim, H. J., Hwang, J. W., Cheong, K. H., Kim, K. A., Cha, H. Y., Lee, J. M., and Kim, C. H. (2016) The dual inhibition of met and EGFR by ME22S, a novel met/EGFR bispecific monoclonal antibody, suppresses the proliferation and invasion of laryngeal cancer. *Ann. Surg. Oncol.* **23**, 2046–2053
26. Patnaik, A., Gordon, M., Tsai, F., Papadopoulos, K. P., Rasco, D., Beeram, M., Fu, S., Janku, F., Hynes, S. M., Gundala, S. R., Willard, M. D., Zhang, W., Lin, A. B., and Hong, D. (2018) A phase I study of LY3164530, a bispecific antibody targeting MET and EGFR, in patients with advanced or metastatic cancer. *Cancer Chemother. Pharmacol.* **82**, 407–418
27. Lee, D., Sung, E. S., Ahn, J. H., An, S., Huh, J., and You, W. K. (2015) Development of antibody-based c-Met inhibitors for targeted cancer therapy. *Immunotargets Ther.* **4**, 35–44
28. Lee, J. M., Lee, S. H., Hwang, J. W., Oh, S. J., Kim, B., Jung, S., Shim, S. H., Lin, P. W., Lee, S. B., Cho, M. Y., Koh, Y. J., Kim, S. Y., Ahn, S., Lee, J., Kim, K. M., *et al.* (2016) Novel strategy for a bispecific antibody: Induction of dual target internalization and degradation. *Oncogene* **35**, 4437–4446
29. Moores, S. L., Chiu, M. L., Bushey, B. S., Chevalier, K., Luistro, L., Dorn, K., Brezski, R. J., Haytko, P., Kelly, T., Wu, S. J., Martin, P. L., Neijssen, J., Parren, P. W., Schuurman, J., Attar, R. M., *et al.* (2016) A novel bispecific antibody targeting EGFR and cMet is effective against EGFR inhibitor-resistant lung tumors. *Cancer Res.* **76**, 3942–3953
30. Labrijn, A. F., Meesters, J. I., de Goeij, B. E., van den Bremer, E. T., Neijssen, J., van Kampen, M. D., Strumane, K., Verploegen, S., Kundu, A., Gramer, M. J., van Berkel, P. H., van de Winkel, J. G., Schuurman, J., and Parren, P. W. (2013) Efficient generation of stable bispecific IgG1 by controlled Fab-arm exchange. *Proc. Natl. Acad. Sci. U. S. A.* **110**, 5145–5150
31. Lobo, E. D., Hansen, R. J., and Balthasar, J. P. (2004) Antibody pharmacokinetics and pharmacodynamics. *J. Pharm. Sci.* **93**, 2645–2668
32. Agarwal, S., Zerillo, C., Kolmakova, J., Christensen, J. G., Harris, L. N., Rimm, D. L., Digiovanna, M. P., and Stern, D. F. (2009) Association of constitutively activated hepatocyte growth factor receptor (Met) with resistance to a dual EGFR/Her2 inhibitor in non-small-cell lung cancer cells. *Br. J. Cancer* **100**, 941–949
33. Jo, M., Stolz, D. B., Esplen, J. E., Dorko, K., Michalopoulos, G. K., and Strom, S. C. (2000) Cross-talk between epidermal growth factor receptor and c-Met signal pathways in transformed cells. *J. Biol. Chem.* **275**, 8806–8811
34. Guo, A., Villen, J., Kornhauser, J., Lee, K. A., Stokes, M. P., Rikova, K., Possemato, A., Nardone, J., Innocenti, G., Wetzel, R., Wang, Y., MacNeill, J., Mitchell, J., Gygi, S. P., Rush, J., *et al.* (2008) Signaling networks assembled by oncogenic EGFR and c-Met. *Proc. Natl. Acad. Sci. U. S. A.* **105**, 692–697
35. Niemann, H. H., Jager, V., Butler, P. J., van den Heuvel, J., Schmidt, S., Ferraris, D., Gherardi, E., and Heinz, D. W. (2007) Structure of the human receptor tyrosine kinase met in complex with the Listeria invasion protein InlB. *Cell* **130**, 235–246
36. Stamos, J., Lazarus, R. A., Yao, X., Kirchhofer, D., and Wiesmann, C. (2004) Crystal structure of the HGF beta-chain in complex with the Sema domain of the Met receptor. *EMBO J.* **23**, 2325–2335
37. Lammerts van Bueren, J. J., Bleeker, W. K., Brännström, A., von Euler, A., Jansson, M., Peipp, M., Schneider-Merck, T., Valerius, T., van de Winkel, J. G. J., and Parren, P. W. H. I. (2008) The antibody zalutumumab inhibits epidermal growth factor receptor signaling by limiting intra- and intermolecular flexibility. *Proc. Natl. Acad. Sci. U. S. A.* **105**, 6109–6114
38. Li, S., Schmitz, K. R., Jeffrey, P. D., Wiltzius, J. J., Kussie, P., and Ferguson, K. M. (2005) Structural basis for inhibition of the epidermal growth factor receptor by cetuximab. *Cancer Cell* **7**, 301–311
39. Cochran, J. R., Kim, Y. S., Olsen, M. J., Bhandari, R., and Wittrup, K. D. (2004) Domain-level antibody epitope mapping through yeast surface display of epidermal growth factor receptor fragments. *J. Immunol. Methods* **287**, 147–158
40. Labrijn, A. F., Meesters, J. I., Priem, P., de Jong, R. N., van den Bremer, E. T., van Kampen, M. D., Gerritsen, A. F., Schuurman, J., and Parren, P. W. (2014) Controlled Fab-arm exchange for the generation of stable bispecific IgG1. *Nat. Protoc.* **9**, 2450–2463
41. Grugan, K. D., Dorn, K., Jarantow, S. W., Bushey, B. S., Pardinas, J. R., Laquerre, S., Moores, S. L., and Chiu, M. L. (2017) Fc-mediated activity of EGFR x c-Met bispecific antibody JNJ-61186372 enhanced killing of lung cancer cells. *MAbs* **9**, 114–126
42. Vijayaraghavan, S., Lipfert, L., Chevalier, K., Bushey, B. S., Henley, B., Lenhart, R., Sendecki, J., Beqiri, M., Millar, H. J., Packman, K., Lorenzi, M. V., Laquerre, S., and Moores, S. L. (2020) Amivantamab (JNJ-61186372), an Fc enhanced EGFR/cMet bispecific antibody, induces receptor downmodulation and antitumor activity by monocyte/macrophage trogocytosis. *Mol. Cancer Ther.* **19**, 2044–2056
43. Yun, J., Lee, S. H., Kim, S. Y., Jeong, S. Y., Kim, J. H., Pyo, K. H., Park, C. W., Heo, S. G., Yun, M. R., Lim, S., Lim, S. M., Hong, M. H., Kim, H. R., Thayu, M., Curtin, J. C., *et al.* (2020) Antitumor activity of amivantamab (JNJ-61186372), an EGFR-MET bispecific antibody, in diverse models of EGFR exon 20 insertion-driven NSCLC. *Cancer Discov.* **10**, 1194–1209
44. Niemann, H. H. (2013) Structural basis of MET receptor dimerization by the bacterial invasion protein InlB and the HGF/SF splice variant NK1. *Biochim. Biophys. Acta* **1834**, 2195–2204
45. Voigt, M., Braig, F., Göthel, M., Schulte, A., Lamszus, K., Bokemeyer, C., and Binder, M. (2012) Functional dissection of the epidermal growth factor receptor epitopes targeted by panitumumab and cetuximab. *Neoplasia* **14**, 1023–1031
46. Haura, E. B., Cho, B. C., Lee, J. S., Han, J.-Y., Lee, K. H., Sanborn, R. E., Govindan, R., Cho, E. K., Kim, S.-W., Reckamp, K. L., Sabari, J. K., Thayu, M., Bae, K., Knoblauch, R. E., Curtin, J., *et al.* (2019) JNJ-61186372 (JNJ-372), an EGFR-cMet bispecific antibody, in EGFR-driven advanced non-small cell lung cancer (NSCLC). *J. Clin. Oncol.* **37**, 9009
47. *Molecular Operating Environment (MOE), 2019.01.* (2021). Chemical Computing Group ULC, 1010 Sherbooke St. West, Suite #910, Montreal, QC, Canada. H3A 2R7
48. Garrett, T. P., McKern, N. M., Lou, M., Elleman, T. C., Adams, T. E., Lovrecz, G. O., Zhu, H. J., Walker, F., Frenkel, M. J., Hoyne, P. A., Jorissen, R. N., Nice, E. C., Burgess, A. W., and Ward, C. W. (2002) Crystal structure of a truncated epidermal growth factor receptor extracellular domain bound to transforming growth factor alpha. *Cell* **110**, 763–773